

Dynamics of transition region loops in an enhanced network simulation of the solar atmosphere

P. Zacharias^{1,2}, V.H. Hansteen^{1,2}, and J. Leenaarts³

¹ Institute of Theoretical Astrophysics, University of Oslo, P.O.Box 1029 Blindern, 0315 Oslo, Norway

² Rosseland Centre for Solar Physics, University of Oslo, P.O. Box 1029 Blindern, NO-0315 Oslo, Norway

³ Institute for Solar Physics, Department of Astronomy, Stockholm University, AlbaNova University Centre, 106 91 Stockholm, Sweden

July 11, 2018

ABSTRACT

Context. The solar chromosphere and transition region are highly dynamic and therefore hard to study. State-of-the art numerical models have now become sufficiently advanced to allow detailed studies of transient events on various scales in space and time.

Aims. The dynamics of cool, low-lying transition region loops and hot, coronal loops are compared. Based on the evolution over several minutes, we are able to characterize various kinds of waves that are travelling along the loops.

Methods. Passive tracer particles (so-called corks) are implemented into a three-dimensional numerical experiment of the solar atmosphere and advected by the plasma flow, while the code is running. By following the cork trajectories, we have a new, highly accurate tool to follow magnetic field lines over time in the simulations.

Results. We compare the evolution of different sets of low-lying and high-reaching loops and present examples of each type. Typical lifetimes of 10–15 min are found for transition region loops, whereas the lifetimes of coronal loops in the model exceed the duration of the simulation span that has been analyzed (25 min). Space-time maps of various plasma parameters give insight on the evolution of the loops in connection with the heating and cooling processes of the plasma. In addition, the decomposition of the velocity vector into components parallel and perpendicular to the magnetic field elucidates the various kind of waves propagating along the magnetic field lines. Magnetoacoustic waves with a frequency of $\sim 0.005 \text{ s}^{-1}$ are omnipresent leading to the swaying of the field lines and their periodic variation in height. Torsional Alfvén waves in the model are often associated with jets of cool plasma that can reach up to 10 Mm in height and last for approximately 10 min. The acceleration force of these cool plasma jets is the combined action of the Lorentz force and the buoyancy force.

Conclusions. Our findings imply that a highly accurate scheme is necessary in order to follow magnetic field lines in time and identify wave-like motions. With a cork-based approach, we are able to identify magneto-acoustic waves as well as Alfvénic waves that are travelling along the magnetic field lines.

Key words. Stars: coronae — Sun: corona — Sun: transition region — Sun: UV radiation — Techniques: spectroscopic

1. Introduction

Coronal loops are considered to be the basic building blocks of the solar corona. Due to the high conductivity and as the magnetic energy dominates over the thermal energy in this region of the Sun's atmosphere, the plasma is confined to field lines channeling the plasma flows. The energy is rapidly distributed along those field lines due to the efficient heat conduction, resulting in loop-like structures aligned with the magnetic field. In the 1970s, it was suggested that magnetic structures rapidly expand into the corona in the form of so-called coronal funnels, which dominate the low corona (Gabriel 1976). As a result of measurements with improved spectral and spatial resolution, it became apparent that the original, simplified picture of the solar atmosphere needed to be modified. Indirect spectroscopic evidence from the High Resolution Telescope Spectrograph (HRTS) and Skylab spectra led to the introduction of the term unresolved fine structure (UFS) by Feldman (1983) and the hypothesis that the plasma in the solar transition region appears in structures

magnetically isolated from the chromosphere and corona. The existence of a multitude of loops of different sizes and temperatures below and between the coronal funnels was suggested by Dowdy et al. (1986), in order to reproduce the correct shape of the emission measure (EM) below 100 000 K. Static, low lying loops were shown to account for the rise of the differential emission measure (DEM) at low temperatures by Antiochos & Noci (1986), however, Cally & Robb (1991) found that such cool loops are thermally unstable. Using transient one-dimensional heating models to investigate the hydrodynamic behavior of small cool magnetic loops, Spadaro et al. (2006) were able to show that small cool structures can produce the observed emission measure distribution and over the entire temperature range, as well as the temperature dependence of the persistent redshifts, provided the heating is spatially localized near the chromospheric footpoints. The high spatial and temporal resolution observations obtained by the Interface Region Imaging Spectrograph (IRIS) have finally revealed observational evidence for the existence of the UFS (Hansteen et al. 2014). These structures are shown

to be short, bright and low-lying varying rapidly on the time scale of minutes. Nowadays, extensive radiative-MHD simulations (Gudiksen et al. 2011) enable full forward-modelling of the solar atmosphere from the convection zone to the corona at a spatial and temporal resolution suitable for comparison with observations (Carlsson et al. 2016). Comparisons with such numerical models showed that low-lying episodically heated loops naturally arise in the state-of-the-art 3D MHD models (Gudiksen et al. 2011; Carlsson et al. 2016), which can thus be used as guidance to exploit their properties in greater detail.

The evolution of the magnetic field lines themselves is rather complex, and the field lines, in general, cannot be thought of as a static background (see, e.g., Leenaarts et al. 2015). In this study, we present results obtained based on a novel technique of following magnetic field lines over time, which is based on the implementation of passive tracer particles in the Bifrost stellar atmosphere code (Zacharias et al. 2018). Whereas earlier approaches have often been limited by the finite time resolution of the snapshot series (typically 10 s cadence), this new approach allows us to follow test particles at highest cadence possible (i.e., timestep cadence of the code) and thus to determine the evolution of the field lines most accurately. We present results from a comparison between low-lying transition region loops and high-reaching coronal loops in a three-dimensional magnetohydrodynamic (3D MHD) experiment of the solar atmosphere above an enhanced network region. The formation and propagation of a cool chromospheric plasma jet, which appears above a strong magnetic field concentration, is found to be associated with the passage of a torsional Alfvén wave, the properties of which are analyzed.

This work is organized as follows. In section 2, the simulations are introduced. Section 3 outlines the new cork method and describes the tracing of the magnetic field lines in time. In section 4, the results of our field line analysis are presented. We conclude this study with a discussion, which puts this work in context with other studies (section 5).

2. Setup of the numerical experiment

The setup of the 3D model is identical to the one described in Zacharias et al. (2018). The simulations have been performed with the Bifrost stellar atmosphere code (Gudiksen et al. 2011), a staggered mesh explicit code that solves the standard MHD partial differential equations on a Cartesian grid, which extends from the upper convection zone to the low corona. The box size is 24x24 Mm² in horizontal direction and \approx 17 Mm in the vertical; it reaches -2.4 Mm below the solar surface and 14.4 Mm above. The simulation has a size of 504x504x496 grid points corresponding to a resolution of \approx 48 km in the horizontal direction. In the vertical direction, a non-equidistant grid spacing is applied, and the resolution ranges between \approx 19 km in the photosphere and transition region to \approx 100 km in the corona, where the temperature and density gradients are less pronounced.

The magnetic field configuration is chosen in a way that it leads to a small network-like configuration. It was created by specifying the magnetic field at the bottom boundary and using a potential field extrapolation to compute the field in the entire computational domain. The magnetic field was inserted into a relaxed hydrodynamical simulation

and was then allowed to evolve freely. The simulation was run for 3000 s of solar time using LTE ionization, before non-equilibrium hydrogen ionization was switched on for 830 s. Afterwards, starting from $t=3850$ s, the simulation was run for 1500 s of solar time without non-equilibrium hydrogen ionization including passive tracer particles. For more details, the reader is referred to Carlsson et al. (2016).

The magnetic field at the bottom boundary consists of two patches of opposite polarity separated by 8 Mm with an overall balanced flux. The average unsigned magnetic field strength in the photosphere is 48 G (5 mT). The magnetic field distribution does not change significantly during the simulation timespan. Both the top and the bottom boundaries are transparent. At the bottom boundary, the magnetic field is passively advected with no extra field fed into the computational domain. The effective temperature of the simulated atmosphere is not set directly, but only indirectly by specifying the incoming entropy flux at the lower boundary. The average temperature in this model is maintained by fluid motions in the convection zone, by radiative transfer in the photosphere, by the balance between acoustic shocks and radiative losses in the lower chromosphere, and by the balance of Joule and viscous heating, thermal conduction, and radiative losses in the upper chromosphere, transition region and corona.

3. Analysis method

Passive tracer particles, so-called corks, have been implemented into the Bifrost simulations (Zacharias et al. 2018). Initially, corks are placed at every point of the simulation grid; we then follow them in time for approximately 25 min. For the tracking of each cork in the simulation, the plasma flow at the respective cork position is considered for every single timestep. The position \mathbf{r}_i of a cork labeled i evolves as $\frac{\partial \mathbf{r}_i}{\partial t} = \mathbf{v}(\mathbf{r}_i)$, where $\mathbf{v}(\mathbf{r}_i)$ is the plasma velocity at the location of the cork. The 3D rMHD simulations thus provide us with a vast number of cork trajectories and a unique tool to trace features, such as individual magnetic field lines, over time.

Fig. 1 shows projections of a magnetic field line on the xz -, yz -, and xy -planes. The field line has been obtained by tracing the magnetic field vector from the cork position, which is indicated by an asterisk. By following the cork trajectory over time, the evolution of the field line is obtained. The corresponding movie (see online material), which shows a swaying motion of a coronal field line, will be discussed in more detail in section 4.2.

The time evolution of various plasma parameters along a field line of length s can be represented by space-time diagrams (see, e.g., Fig. 4). The st -panels show the evolution of plasma temperature T and density ρ in the first row; plasma- β , field line curvature κ and torsion τ in the second row; plasma flow speed parallel to the field line $u_{\parallel} = \mathbf{u} \cdot \mathbf{b}$ and the two transverse directions $u_P = \mathbf{u} \cdot \mathbf{P}$ and $u_N = \mathbf{u} \cdot \mathbf{N}$ in the third row. This representation makes it easy to distinguish between disturbances propagating along or perpendicular to the magnetic field. In the fourth row, we show the divergence of the plasma flow parallel to the magnetic field ($\nabla_{\parallel} \cdot \mathbf{u} = \partial u_{\parallel} / \partial s$), the divergence of the flow field perpendicular to the field ($\nabla_{\perp} \cdot \mathbf{u} = \nabla \cdot \mathbf{u} - \partial u_{\parallel} / \partial s$) and the vorticity parallel to the magnetic field. The fifth row shows the evolution of the adiabatic heating rate

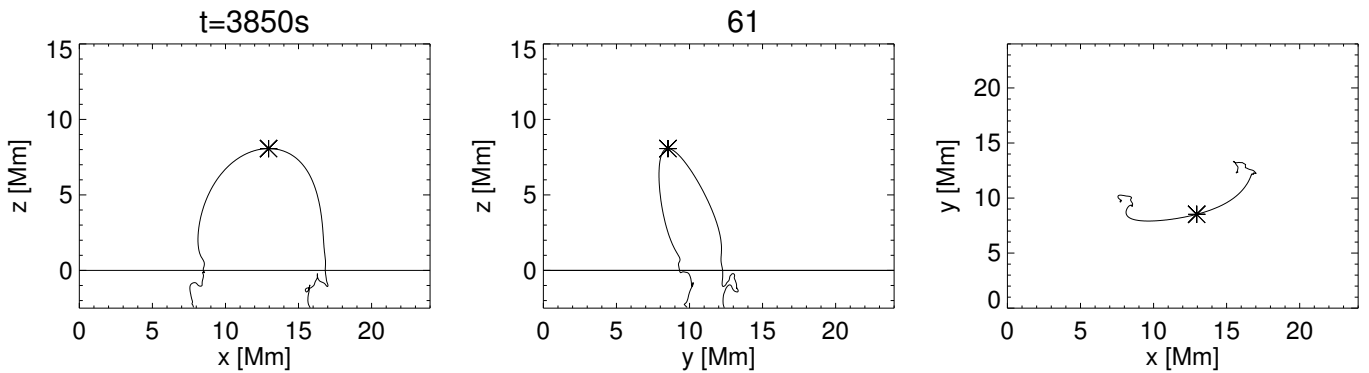


Fig. 1. Example of swaying field line. A movie showing the temporal evolution of the field line is found in the appendix.

(Q_{pdV}), the Joule heating rate (Q_{Joule}), and the viscous heating rate (Q_{visc}) per particle along the field line.

In the following, we are focusing on a time sequence of about 25 minutes duration in the numerical experiment. All points of time discussed here refer to time $t=0$ at the beginning of this sequence. This is the time, when the corks are implemented into the simulation. The actual simulation was started long before $t=0$, so that any impact of the initial condition is excluded during the investigated time sequence.

4. Results

We start this section with a discussion on the importance of using corks for the field line tracing (section 4.1). We then focus on two different sets of magnetic field lines, namely coronal field lines (section 4.2) and transition region field lines (section 4.3), and investigate their properties and their temporal evolution during the simulation. In particular, we analyze the various kinds of waves that are found to propagate along these loops. In section 4.4, we study the evolution of a field line bundle, which is associated with a cool plasma ejection and an Alfvénic wave.

4.1. Field line advection algorithms

The importance of an accurate field line tracing algorithm becomes clear when comparing the two approaches described below. Field line advection algorithms, such as the one provided by the Visualization and Analysis Platform for Ocean, Atmosphere, and Solar Researchers (VAPOR, Clyne & Rast 2005; Clyne et al. 2007) typically suffer from the ambiguous behaviour of the plasma flow between consecutive snapshots of a time-series.

VAPOR supports the option to follow magnetic field lines under the influence of a velocity field, however, it can only do so at timestep cadence (typically 10 sec). The implemented field line advection algorithm is representative for methods that are typically used to follow magnetic field lines in simulations. It is based on the following steps: (1) Specification of a set of seed points for the steady (magnetic) field at a starting time t_0 . (2) Integration of seed points in the magnetic field results in a set of field lines. (3) Along each field line, the point with the strongest magnetic field is selected (*i.e.*, the photospheric footprint). (4) These points are advected in the velocity field to the next

time step t_1 and used as seeds for the next timestep. (5) Steps 2-4 are repeated for each subsequent timestep t_n .

In the following, we compare the evolution of a set of magnetic field lines obtained with the VAPOR field line advection algorithm (Fig. 2, top row) with that obtained from the cork trajectories (Fig. 2, bottom row). Magnetic field lines have been traced for 20 minutes, however, we find large discrepancies for the two approaches after only a few minutes. The field lines, which were obtained by using the corks, tend to accumulate and appear in bundles, whereas the field lines, which are based on the field line advection algorithm, tend to spread out and distribute more evenly. Clear differences become evident after ~ 2 minutes. Some of the field lines, which have been followed in time by using the cork approach, in particular the ones that are high-reaching, form a cusp shape at their top. This behavior is not found for the field lines obtained through the field line advection algorithm. In general, the latter field lines appear more disperse and less bent or twisted. These discrepancies are due to the higher temporal resolution inherent to the cork approach, which allows to follow the plasma flows as accurately as possible, whereas the field line advection algorithm is limited by the snapshot cadence, and no information on the plasma flows is provided in between snapshots.

4.2. Magnetic field line evolution - coronal loops

Figure 3 shows the evolution of a bundle of coronal field lines, which connect the two main magnetic polarities centered at approximately $(x, y)=(7.5, 13.5)$ Mm and $(x, y)=(15.5, 11.5)$ Mm. The field line bundle was derived by tracing corks that are initially located at a height of 8.3 Mm. Shown in red is the emission of the optically thin OVI (1031Å) line, which has been calculated by employing the CHIANTI atomic database (Dere et al. 1997; Landi et al. 2013). The field lines are shown to roughly outline the emission at upper transition region temperatures.

The corresponding *st*-diagrams of one of these field lines is shown in Fig. 4. Only the part of the field line above the photosphere is shown. The position along the loop is started from the right footpoint (see upper left panel). The second footpoint of the loop is marked by a white or black line depending on the respective panel. Initially, the loop is 22 Mm long, and a large fraction of the loop has coronal temperatures. Only a small part close to the loop footpoints is chromospheric. During the first 6 min, the loop length

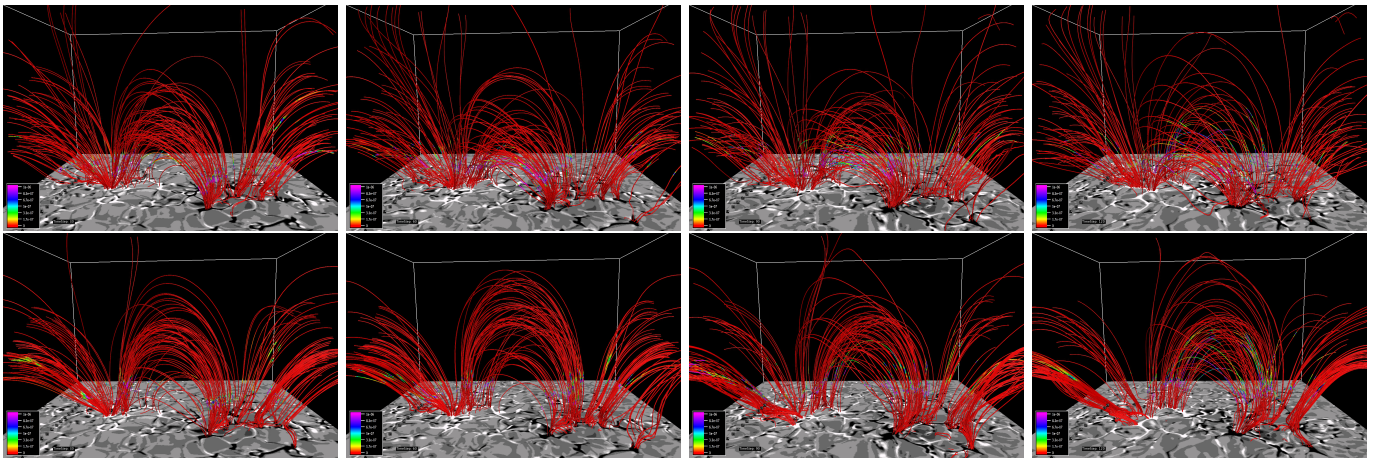


Fig. 2. Comparison of evolution of magnetic field lines obtained by using the VAPOR field line advection algorithm (top row) and the cork trajectories (bottom row). See section 3 for more details. From left to right, snapshots are shown for $t=300$ s, 600 s, 900 s and 1200 s. Scaling of vertical magnetic field at the solar surface ($z=0$ Mm) is from -100 G to +100 G.

increases to ~ 33 Mm, and the loop apex rises in height from approximately 8 Mm to 13 Mm. The temperature and pressure panels show that, while the field line expands and the plasma pressure decreases, the upper part of the loop is cooling. After the initial rising phase, the loop length varies only slightly with a period of roughly 200 s due to the passage of slow-magnetoacoustic waves.

Both loop footpoints are sources of slow-mode waves, and the latter are found to propagate along the entire length of the field line (see *e.g.*, u_{\parallel} and $\text{div } u_{\parallel}$ panel, Fig. 4). Once the waves reach the transition region, they are either reflected and/or they steepen considerably and continue to travel at much higher speed along the field line. Both normal velocity components, u_P and u_N , show transverse oscillations running at Alfvén speed along the field line in both directions and causing an interference pattern with complex apparent phase speeds. Note that the Alfvén crossing time for a coronal field line of length 30 Mm is ~ 60 s only, assuming a propagation speed of 500 km/s, but it can be as low as 15 s for a propagation speed as high as 2000 km/s along certain parts of the field line, so that the propagation is barely resolved in our time-series of 10 s cadence.

4.3. Magnetic field line evolution - low-lying loops

The right panel in Fig. 3 shows a bundle of low-lying field lines that have been traced by following corks in the range $x=[12.5,13.5]$ Mm, $y=[14.5,15.5]$ Mm, and $z=4.3$ Mm at $t=3850$ s. The loops are found to connect the two main magnetic polarities and to outline a region that appears bright in CIV (1548Å) emission for several minutes.

At the start of the simulation, the field lines of the bundle vary between 4.3 and 4.8 Mm in height and between ~ 13 and ~ 15 Mm in length. Despite their similar sizes, a great range of apex temperatures ($T_{\text{apex}}=10\,000\text{--}700\,000$ K) is observed among these loops. In the following, we will focus on the two most common categories, *i.e.*, (1) cool loops with an initial apex temperature of less than $T=30\,000$ K (see Fig. 5) and (2) hot loops with initial apex temperature above $T=300\,000$ K (see Fig. 6). During the first 5 min, the hot loops quickly grow in length, before they abruptly shrink and regain their initial size, whereas the cool loops

retain roughly the same height throughout their existence. The cool loops exist for 600–800 s; they reach typical transition region temperatures ($T=\dots$ K), when they undergo heating. In the following, we will discuss how the two kinds of loops differ and what causes them to change their structure after a few minutes.

Fig. 5 shows the evolution of a field line with a rather cool loop apex ($T_{\text{apex}}=12\,000$ K), which gets heated slowly to transition region temperatures ($T_{\text{apex}}=300\,000$ K) within ~ 400 s. It remains in this state for approximately 400 s, before it quickly cools to temperatures below 10 000 K. The loop size is found to vary between 10 and 13 Mm during the first 800 s, and the sound speed, which depends on the square root of the temperature, increases from ~ 20 km/s to ~ 110 km/s in the upper part of the loop as the temperature rises. The Alfvén speed, on the other hand, shows a much larger variation. At the apex of the field line, it increases over time from ~ 450 km/s at $t=0$ s to ~ 650 km/s at $t=400$ s, as the density along the field line decreases. The effect is most dramatic in the right leg of the field line, where the Alfvén speed increases from ~ 900 to ~ 1800 km/s during the same time, as the density drops by roughly an order of magnitude.

The field line above the right loop footpoint becomes increasingly **bent and twisted** between $t=600\text{--}790$ s (see Fig. ??), and the height of the loop apex decreases from 4.5 to 2.8 Mm. Consequently, the loop shrinks in size by a considerable fraction. This phase is associated with the passage of a torsional Alfvén wave, signatures of which are most clearly seen in the space-time maps of τ , u_N , u_P and $\text{curl } u_{\parallel}$ in Fig. 5 between $t=600$ s and $t=800$ s. **As discussed in the example shown in section 4.4, the Alfvén wave is associated with a cool plasma jet, which propagates along the field line.** The passage of the torsional Alfvén wave leads to a strong velocity signal in the directions perpendicular to the magnetic field line and to a significant shift of the field line apex in x -, y - and z -direction at $t=720$ s (see Fig. ??, left panel). Eventually, the **twist** along the field line is released, and the field line changes to a new, lower lying configuration and a much lower temperature state (see Fig. 5). **We consider this the end of the previously existing field line.** A second discontinuity appears shortly afterwards, be-

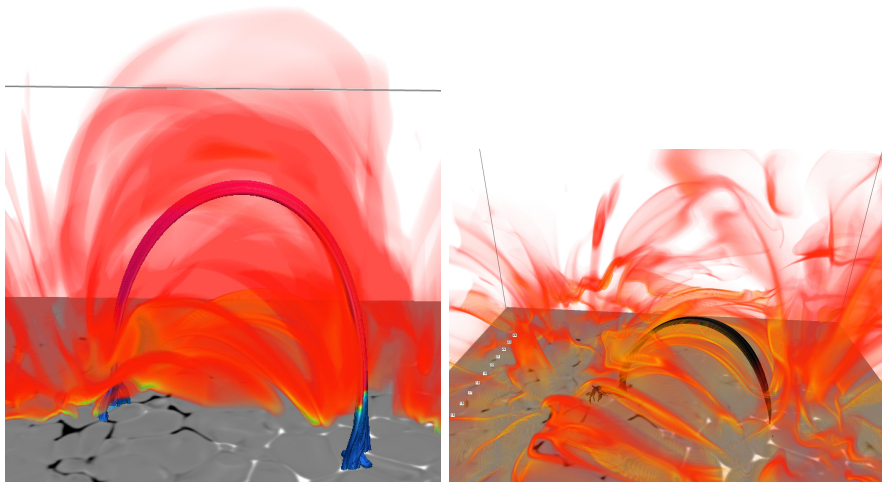


Fig. 3. *Left panel:* Bundle of coronal field lines and synthesized OVI (1031Å) emission. The field lines are traced from corks placed on an equidistant grid in the range $x=[12.5,13.5]$ Mm, $y=[8.5,9.5]$ Mm and $z=8.3$ Mm. They are color-coded according to $\log T$ (dark blue $T=2\,000$ K, light blue: $T=12\,000$ K, green: $T=30\,000$ K, yellow: $T=60\,000$ K, red: $T=100\,000$ K, pink: $T > 1\,000\,000$ K). *Right panel:* Low-lying field line bundle extracted from corks at a height $z=4.3$ Mm. In addition, the synthesized CIV (1548Å) emission at $t=3850$ s is shown. The viewing direction is from the side, approximately in y -direction. In addition, the vertical magnetic field strength at $z=0$ Mm is shown; the scaling is -1.5kG (black) to +1.5kG (white).

tween 790 s and 800 s, as the Alfvénic wave reaches the loop apex and causes another change in field line geometry leading to yet another unbending of the field line (see Fig. ??, left panel and Fig. ??).

The second example (Fig. 6) shows a rather hot ($T_{\text{apex}}=500\,000$ K) field line that expands in length from 15 to 22 Mm during the first 5 minutes and then quickly shrinks to ~ 15 Mm within 30 seconds. It remains at an average length of ~ 12 Mm for the remainder of the time-series. The loop expansion is driven by strong upflows in both loop legs, which appear as black and white patches in the u_{\parallel} panel. During this phase, strong Joule heating and a strong temperature increase are observed, in particular in the left loop leg (see Fig. 6), and the field line becomes increasingly bent above the right loop footpoint. At $t=330$ s, the field line unbends and reverts to a more compact shape similar to the initial configuration (see Fig. ??, right panel). A significant drop in height of both the apex and the cork are observed. At the same time, flow speeds along the loop are reversed and strong draining of material is observed along the entire upper part of the loop (again visible as white and black patches in the u_{\parallel} panel). In addition, both loop footpoints are shifted by a significant amount. The field line contracts and regains a more symmetric shape. The shrinking of the loop is accompanied by strong adiabatic heating, as well as Joule and viscous heating. Shortly afterwards, it is found in a much hotter, coronal-like temperature state, where it remains for approximately 500 s.

The constant swaying of the field line due to the passage of magnetoacoustic waves leads to periodic changes of the field line height on a timescale of approximately 200 s. In addition, the field lines are constantly shaken by Alfvénic waves, which are evident as periodic signatures travelling at Alfvén speed along the lines in the u_N and u_P panels. A strong torsional signal is found to propagate upwards along the field line between 650-800 s (Fig. 6), which results in the field line above the right footpoint getting strongly bent (see Fig. ??). The sudden release of this twist at $t=800$ s, as the wave has passed, marks the end of the hot-temperature-phase of this particular field line.

What are the similarities between these two lines: lifetime, initial size (length & height) and position (not temperature), ...

Accordingly, the apex sound speed varies between 90 km/s ($t=200$ s), 180 km/s ($t=400$ s), 150 km/s ($t=600$ s), 100 km/s ($t=800$ s), 40 km/s ($t=1000$ s), and 20 km/s

($t=1200$ s), whereas Alfvén speed at the top of the loop varies between 2100 km/s in the first half and 800 km/s in the second half of the time series.

4.4. Cool plasma jets

In the lower right corner of the simulation box ($x=20$ -24 Mm and $y=2$ -8 Mm), several cool plasma jets occur between ~ 600 and 1000 s after the injection of the corks. These cool jets with temperatures well below 10 000 K travel with speeds of approximately 50-60 km/s and reach heights of up to 8 Mm. They are found to last for approximately 10 minutes.

In Fig. 7, a time-sequence of such a jet is shown together with a bundle of magnetic field lines that are rooted within a strong magnetic flux concentration (shown by the white patch in the underlying magnetogram). The different panels show the evolution of temperature in a small section of the simulation box ($\sim 5 \times 2 \times 10$ Mm). The magnetic field lines, which roughly outline the path of the jet, are color-coded according to the respective plasma temperature. This particular plasma jet is found to move upwards between $t=660$ s and $t=840$ s; it lasts for roughly 600 s. It is most clearly seen in the space-time maps of temperature and density in Fig. 8. **Here we can see that the ejection of the jet already starts around $t=5000$ s.** The ejection is connected to the passage of a torsional Alfvén wave (see Fig. 8, panels τ , u_N , u_P and $\text{curl } u_{\parallel}$), the evolution of which is depicted in Fig. 7. The wave is visible as an upwards propagating rotational motion along the field line bundle.

To clarify the acceleration process of the cool plasma jet, an evaluation of the vertical components of the momentum equation has been performed. Fig. 9 shows that a combination of buoyancy force ($F_B = -\frac{1}{\rho} \frac{\partial p}{\partial z} + g_z$) and Lorentz force ($F_L = \frac{1}{\rho} [(\nabla \times \mathbf{B}) \times \mathbf{B}]_z$) leads to a strong upwards pointing force at $z=0.1$ -0.2 Mm along the loop between $t=4800$ and 5000 s. This combined force leads to an upwards travelling disturbance of ~ 14 km/s (see Fig. 9, bottom right panel).

As pointed out in section 4.3 (Fig.s 5 and 6), the correlation between cool plasma being propelled upwards and torsional Alfvénic waves is a process commonly encountered in transition region and coronal loops...

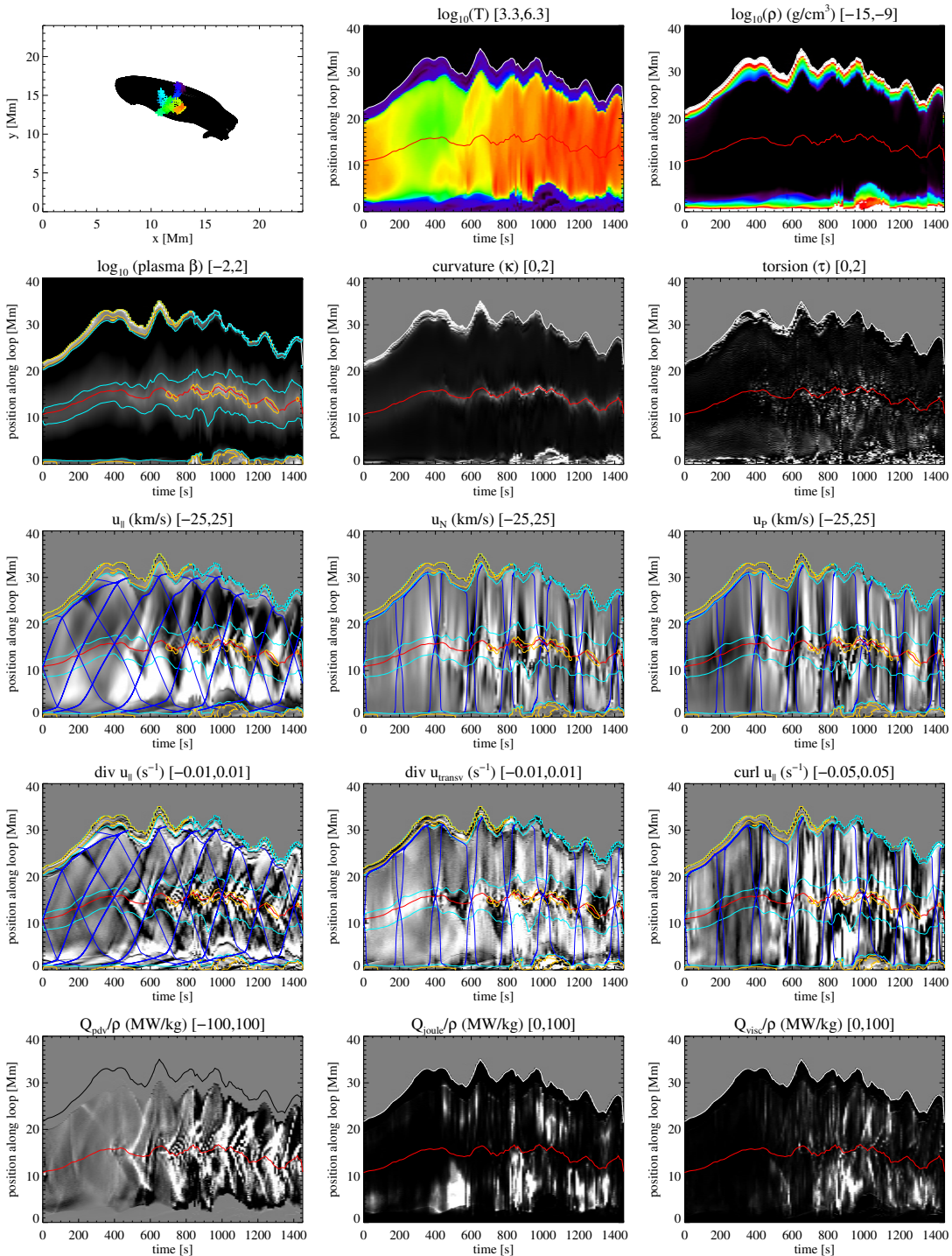


Fig. 4. Evolution of a coronal field line. The upper left panel shows a top view of the computational domain, with the location of the field line at different timesteps. The corks from which the field lines have been extracted are marked by an asterisk. The evolution is from dark blue ($t=0$ s) to red ($t=1450$ s) colors. The other panels show space-time diagrams of different plasma parameters, where the time-evolution (x -axis) is shown as a function of loop-length s (y -axis). The displayed quantity and its range are given above each panel. The zero point of s is the intersection of the field line with the $z=0$ Mm plane, where \mathbf{b} points upward. The field line apex is marked by a red line, the second footpoint is indicated by a white or black line. The orange and light blue curves indicate the plasma- $\beta=1$ and 0.1 values. The blue curves show the wave trajectories, *i.e.*, the path of a signal propagating at wave speed along the loop. The wave speed is the sound speed in panels labeled u_{\parallel} and $\text{div } u_{\parallel}$ and the Alfvén speed for panels u_N , u_P , $\text{curl } u_{\parallel}$. For this particular example, $\text{div } u_{\text{transv}}$ shows both, signals propagating at sound speed and Alfvén speed.

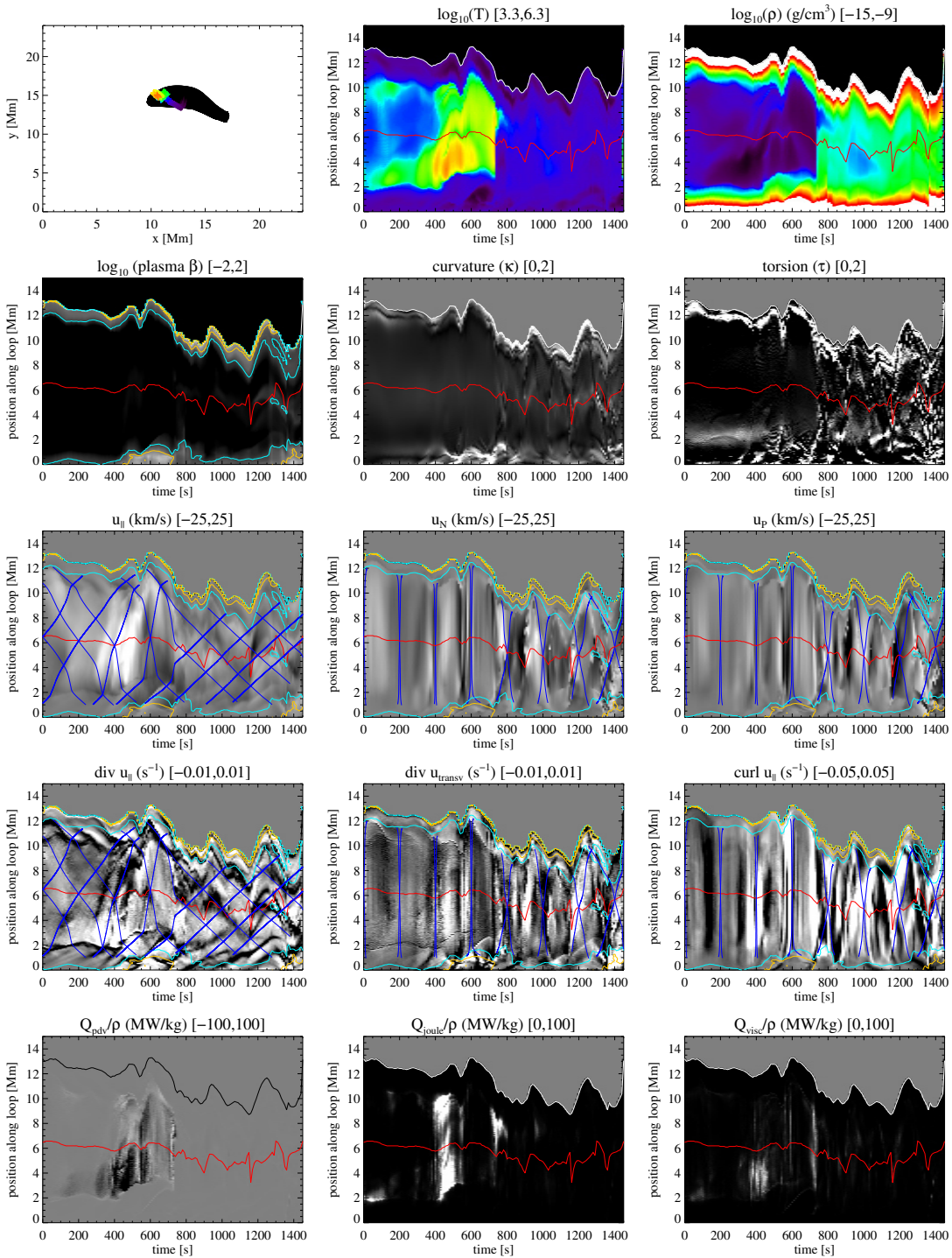


Fig. 5. Space-time maps showing the evolution of a low-lying transition region loop (line 488). See Fig. 4 for a description of the various panels.

5. Discussion

Transition region loops exhibit a much more dynamic structure compared to coronal loops. They are found to quickly evolve between different equilibrium states on the time-scale of 10-15 minutes. This arises quite naturally from the highly dynamic structure of the solar transition re-

gion. In this study, we have compared the dynamics of these low-lying transition region loops to the dynamics of high-reaching coronal loops in an enhanced network simulation following our new cork-based approach of tracing magnetic field lines over time.

The strength of the cork-based approach to follow the evolution of the magnetic field lies in the fact that it takes

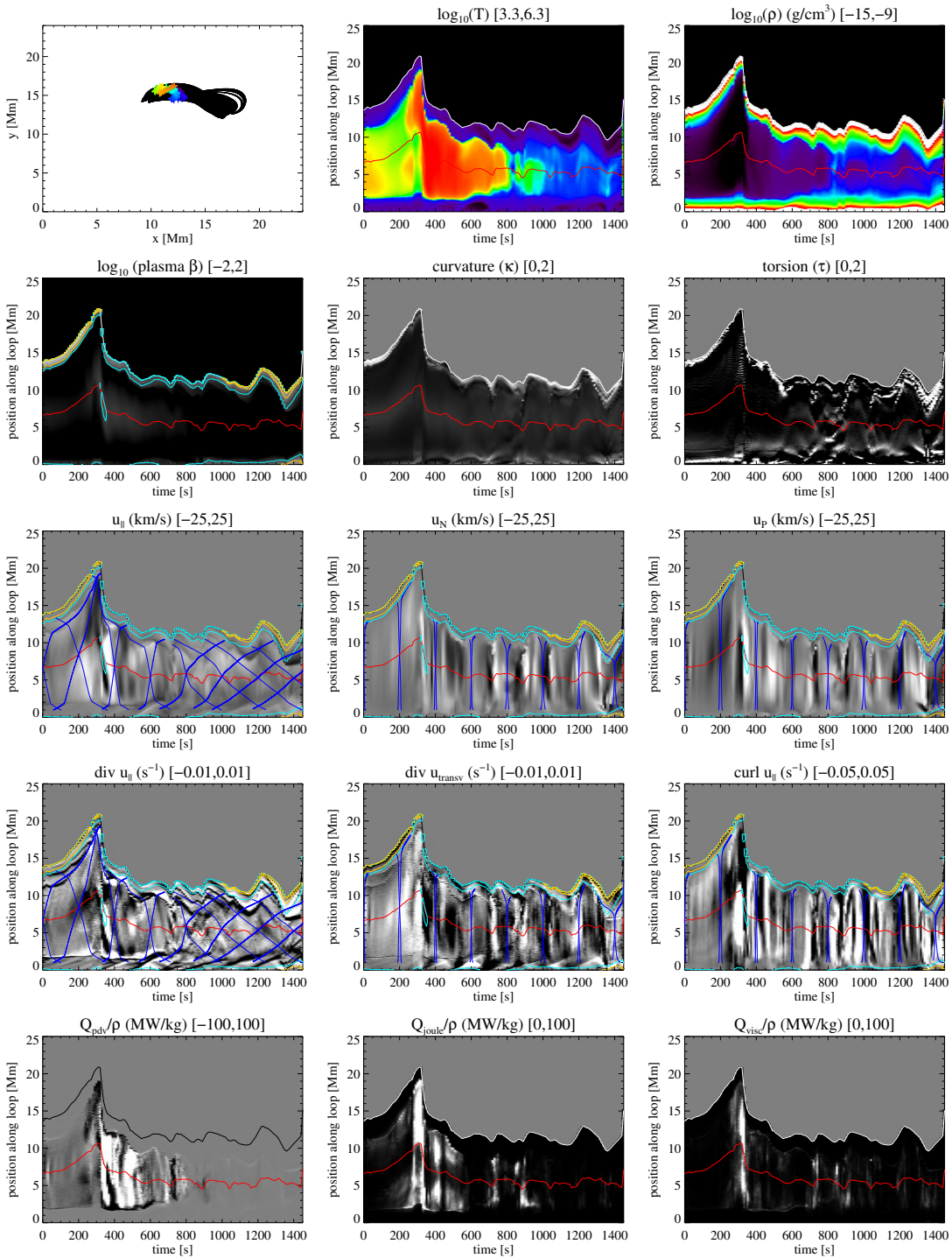


Fig. 6. Space-time maps showing the evolution of a transition region loop (line 5). See Fig. 4 for a description of the various panels.

into account motions that happen on very small timescales, *i.e.*, timescales below the typical snapshot cadence of 10 seconds. In that way, a very accurate picture of the plasma flow evolution can be obtained.

Quite naturally, a field-line-based analysis approach only brings forward waves that travel parallel to the magnetic field. Fast mode waves can propagate at an angle

to the magnetic field and cannot be easily identified with this approach. Even though these waves are expected to be present in the simulations, no efforts have been undertaken to identify them in this study.

The comparison between low-lying transition region and larger coronal loops gives important insights on the evolution of the plasma parameters dynamics along and also

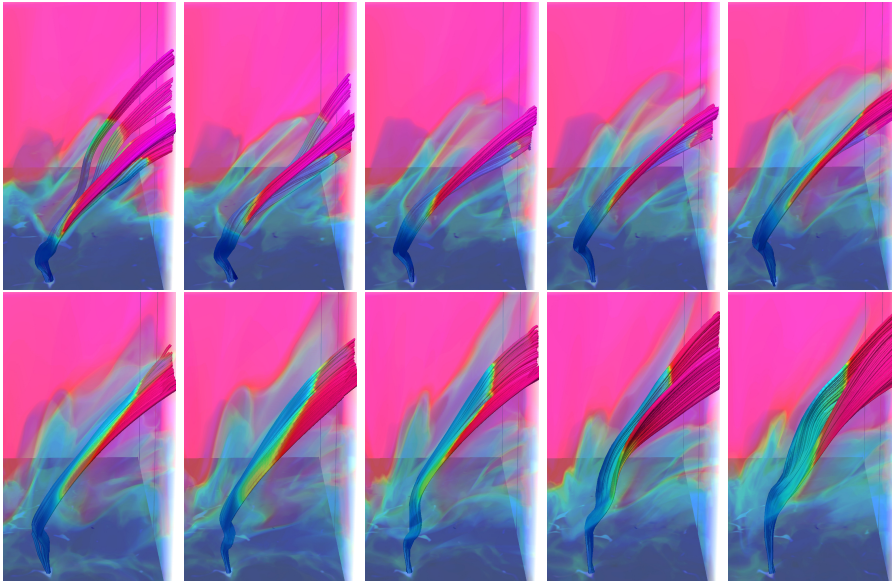


Fig. 7. Trajectories of a cool plasma jet and evolution of a co-aligned bundle of magnetic field lines. The evolution between $t = 660 - 840$ s (see section 4.4). The snapshots shown are 20 s apart. The temperature in a small box of size $5 \times 2 \times 10$ Mm is presented by the following colors: dark blue $T = 2000$ K, light blue: $T = 12\,000$ K, green: $T = 30\,000$ K, yellow: $T = 60\,000$ K, red: $T = 100\,000$ K, pink: $T > 1\,000\,000$ K. The field lines are also color-coded by the respective temperature. A torsional Alfvén wave is found to propagate upwards.

on their lifetimes. Thus, based on the results shown here and on larger statistical studies that were performed on the same dataset and will be published in a follow-up paper, we find that transition region loops (...) have typical lifetimes of only 10-15 minutes in enhanced network regions.

Let's move this to the discussion! Recently, Iijima & Yokoyama (2017) presented a three-dimensional simulation of chromospheric jets. The magnetic field lines in their model are strongly entangled in the chromosphere. The chromospheric jet is driven by the Lorentz force and exhibits oscillatory motion as a natural consequence of its generation mechanism. Their results imply a close relationship between the simulated jet and solar spicules.

Let's move this to the discussion! van Ballegooijen et al. (2017) suggested that coronal loops and the underlying chromosphere may both be heated by Alfvénic turbulence. The authors employ a 3D MHD model for the propagation and dissipation of Alfvén waves in a coronal loop using the reduced MHD approximation. The increase of Alfvén speed with height in the chromosphere and transition region (TR) causes strong wave reflection, which leads to counter-propagating waves and turbulence in the photospheric and chromospheric parts of the flux tube. Part of the wave energy is transmitted through the TR and produces turbulence in the corona. In their model, hot coronal loops typically found in active regions can be explained in terms of Alfvén wave turbulence, provided that the small-scale footpoint motions have velocities of 1-2 km/s and timescales of 60-200 s.

6. Outlook

Acknowledgements. We have used VAPOR (Clyne & Rast (2005), Clyne et al. (2007)) extensively for visualisations. CHIANTI is a collaborative project involving George Mason University, the University of Michigan (USA) and the University of Cambridge (UK).

References

- Antiochos, S. K. & Noci, G. 1986, ApJ, 301, 440
- Cally, P. S. & Robb, T. D. 1991, ApJ, 372, 329
- Carlsson, M., Hansteen, V. H., Gudiksen, B. V., Leenaarts, J., & De Pontieu, B. 2016, A&A, 585, A4

- Clyne, J., Mininni, P., Norton, A., & Rast, M. 2007, New Journal of Physics, 9, 301
- Clyne, J. & Rast, M. 2005, in Electronic Imaging 2005, International Society for Optics and Photonics, 284–294
- Dere, K. P., Landi, E., Mason, H. E., Monsignori Fossi, B. C., & Young, P. R. 1997, AASS, 125, 149
- Dowdy, Jr., J. F., Rabin, D., & Moore, R. L. 1986, Sol. Phys., 105, 35
- Feldman, U. 1983, ApJ, 275, 367
- Gabriel, A. H. 1976, Philosophical Transactions of the Royal Society of London Series A, 281, 339
- Gudiksen, B. V., Carlsson, M., Hansteen, V. H., et al. 2011, A&A, 531, A154
- Hansteen, V., De Pontieu, B., Carlsson, M., et al. 2014, Science, 346
- Iijima, H. & Yokoyama, T. 2017, ApJ, 848, 38
- Landi, E., Young, P. R., Dere, K. P., Del Zanna, G., & Mason, H. E. 2013, ApJ, 763, 86
- Leenaarts, J., Carlsson, M., & Rouppe van der Voort, L. 2015, ApJ, 802, 136
- Spadaro, D., Lanza, A. F., Karpen, J. T., & Antiochos, S. K. 2006, ApJ, 642, 579
- van Ballegooijen, A. A., Asgari-Targhi, M., Cranmer, S. R., & DeLuca, E. E. 2017, ApJ, 736, 3
- Zacharias, P., Hansteen, V. H., Leenaarts, J., Carlsson, M., & Gudiksen, B. V. 2018, A&A, 614, A110

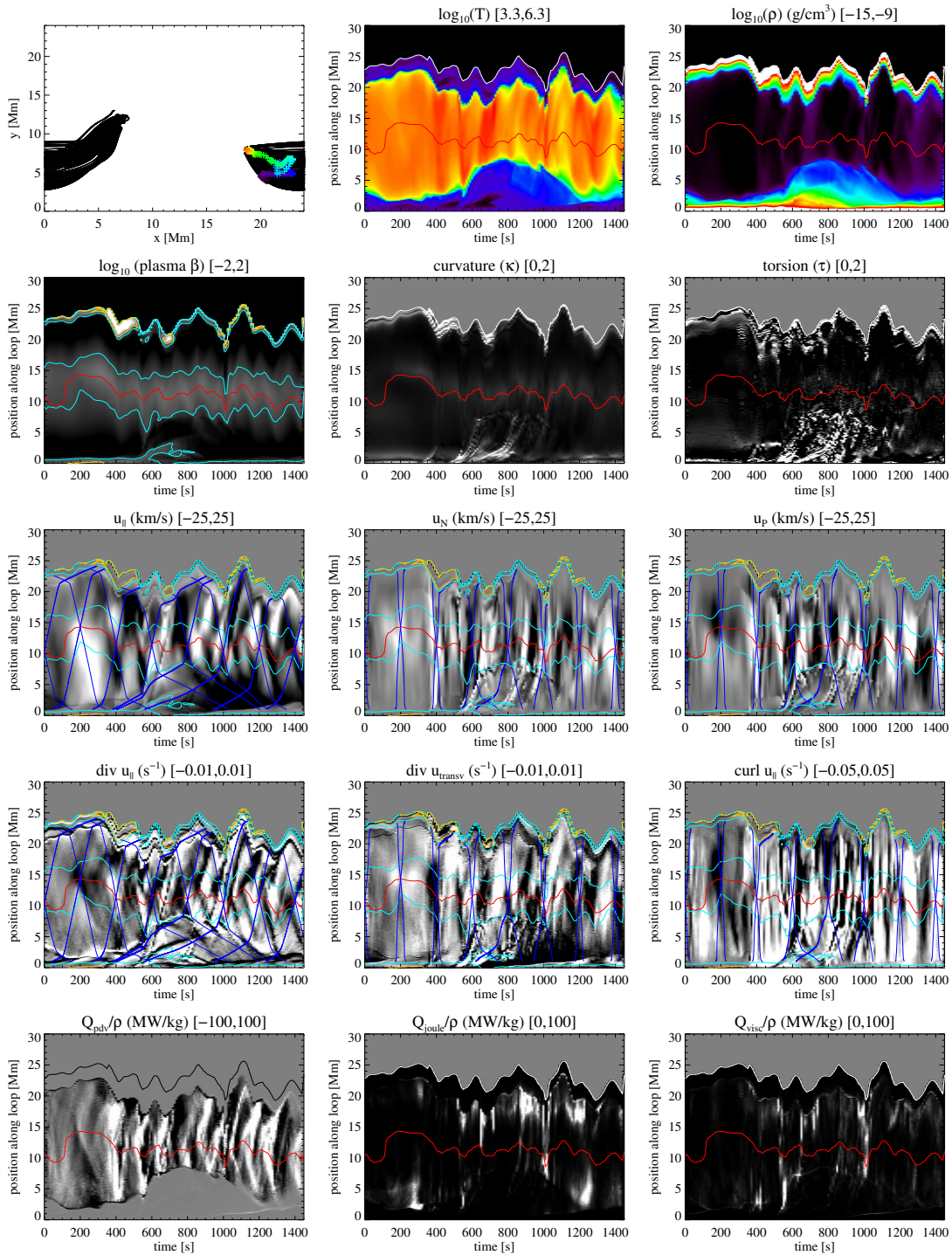


Fig. 8. Space-time maps of line 9, which shows a cool plasma ejection between $t=600-1000$ s (see section 4.4). See Fig. 4 and section 4.1 for an explanation of the various panels.

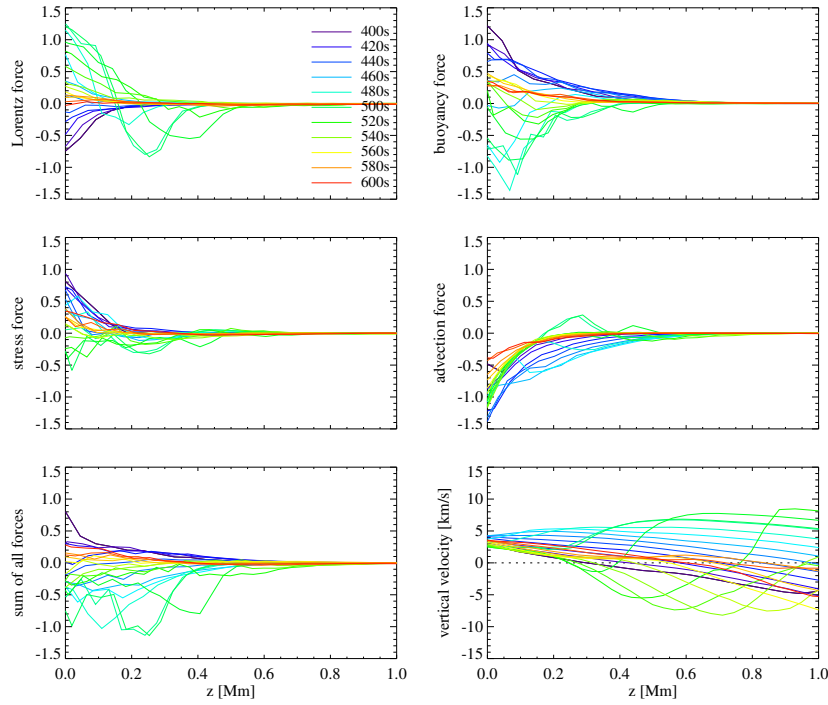


Fig. 9. Evolution of individual force terms acting on the plasma along the loop shown in Fig. 11. Only low heights between 0 and 1 Mm of the loop are considered. The sum of all force terms is shown in the bottom row together with the vertical velocity.